Assessing Uncertainties in Mass Balance Estimation Using the Input-Output Method: A Case Study Around the Wilkes Land

Guojun Li ^{1, 2}, Tong Hao ^{1, 2}, Zhongbo Huang ^{1, 2}, Chen Lv ^{1, 2}, Liang Tang ^{1, 2}, Shi Li ^{1, 2}, Xiangbin Cui ³, Bo Sun ³, Kenichi Matsuoka ⁴, Rongxing Li ^{1, 2}

College of Surveying and Geo-Informatics, Tongji University, 1239 Siping Road, Shanghai, China
China Polar Research Institute of China, Shanghai 200136, China - (cuixiangbin@pric.org.cn, sunbo@pric.org.cn)
Norwegian Polar Institute, Tromsø, Norway - Kenichi.Matsuoka@npolar.no

Keywords: Input-output method, Discharge, Ice thickness, Ice velocity, Uncertainty.

Abstract

Accurate assessment of Antarctic mass balance is essential for understanding and projecting sea-level rise. In this study, we assess the uncertainties in mass balance estimates using the input—output method in Wilkes Land, East Antarctica, with a focus on Basin 13. We developed a new flux gate product based on enhanced radar echo sounding (RES) coverage from Bedmap1, Bedmap2, and Bedmap3, enabling placement closer to the grounding line and reducing spatial bias. Using five different ice thickness datasets (Bedmap2, Bedmap3, BedMachineV2, BedMachineV3, and RES-derived thickness) along with velocity maps from 1995 to 2022, we calculate ice discharge and quantified the associated uncertainties. The results show that the improved flux gate and high-accuracy thickness data reduced discharge uncertainty from 53% to 4%. Approximately 42% of this reduction was due to improved thickness data, while about 7% resulted from the use of higher-quality velocity datasets. These findings highlight the essential role of accurate flux gate placement and reliable thickness data in reducing uncertainties in input—output-based Antarctic mass balance estimates.

1. Introduction

The Antarctic Ice Sheet (AIS) holds approximately 58 m of sealevel equivalent (SLE) ice (Shepherd et al., 2018), with the East Antarctic Ice Sheet (EAIS) accounting for about 52 m (Morlighem et al., 2020). Over recent decades, AIS has exhibited a net mass loss, with West Antarctica Ice Sheet (WAIS) being the dominant contributor to this trend (Otosaka et al., 2023). In contrast, the EAIS has traditionally been regarded as more stable and less sensitive to ocean-climate interactions (Stokes et al., 2022). Some studies have even suggested a slight mass gain in the EAIS, though with substantial uncertainty (Shepherd et al., 2018). However, several studies suggest that certain regions of the EAIS, particularly marine-based basins in Wilkes Land, may be more susceptible to ocean-driven change than previously thought (Li et al., 2023; Stokes et al., 2022).

Wilkes Land has attracted increasing scientific interest due to its extensive subglacial basins, many of which lie below sea level and are in direct contact with warm ocean waters (Morlighem et al., 2020). These characteristics make the region particularly vulnerable to basal melting and dynamic thinning (Adusumilli et al., 2020; Smith et al., 2020). Basin 13 in Wilkes Land, which includes major outlet glaciers such as Totten, Moscow University, Holmes, and Frost, is among the most dynamically active areas in East Antarctica. Together, these glaciers contribute one of the highest ice discharge rates among the 27 defined Antarctic basins (Zwally et al., 2012). Given its dynamic behavior and potential impact on sea level rise, Basin 13 serves as the focus of this study.

The input-output (IO) method is one of the primary approaches for estimating Antarctic mass balance (Gardner et al., 2018; Rignot et al., 2019). This method partitions mass balance into two

primary components: surface mass balance (SMB), representing net precipitation over the interior, and ice discharge, representing the ice across the grounding line (Li et al., 2024). SMB is generally derived from high-resolution regional climate models, such as RACMO (Van Wessem et al., 2014, 2018), while ice discharge is calculated using ice velocity and thickness datasets. Because ice discharge is directly linked to ice dynamics and sealevel contributions, accurately capturing this term is essential for understanding both current and future ice sheet behavior. However, discharge estimates still face large uncertainties, mainly due to limited coverage of the high accuracy thickness and velocity data around the grounding line.

Recent advances in radar surveys have significantly improved the coverage and accuracy of ice thickness data. Gridded datasets such as Bedmap2 (Fretwell et al., 2022), Bedmap3 (Pritchard et al., 2024), BedMachineV2 (Morlighem, et al., 2020), and BedMachineV3 (Morlighem, 2022) integrate a variety of measurements, with radar echo sounding (RES) providing the most precise point-based thickness observations (Gardner et al., 2018). Meanwhile, velocity products such as MEaSUREs (Rignot, 2017) and ITS_LIVE (Gardner et al., 2019) have extended the temporal coverage of surface velocity observations back to the 1990s, enabling multi-decadal analyses of glacier dynamics.

Despite these improvements, many of the RES thickness measurements remain sparse near grounding lines, which are critical locations for discharge calculation. To overcome this limitation, researchers commonly place an inland flux gate at a location where ice thickness are more accuracy to allow reliable ice flux estimates. Discharge between the grounding line and the flux gate is then corrected base on mass conservation (Gardner et

¹ Center for Spatial Information Science and Sustainable Development, Tongji University, 1239 Siping Road, Shanghai, China – (liguojunlee@tongji.edu.cn, tonghao@tongji.edu.cn, 2411749@tongji.edu.cn, carolina@tongji.edu.cn, 2818972208@qq.com, 863546013@qq.com, rli@tongji.edu.cn)

al., 2018). Since SMB corrections generally account for more than 95% of the necessary adjustment (Cheng et al., 2023), this study applies SMB-only corrections. Furthermore, as newer RES surveys have filled gaps in coastal regions (Pritchard et al., 2025), we generate an updated flux gate configuration located closer to the grounding line. This refinement reduces the reliance on corrections and enhances discharge accuracy.

In this study, we reassess the mass balance of the Wilkes Land region by integrating multiple datasets and refining the placement of the flux gate. We generate five discharge time series covering the period from 1995 to 2022 using various combinations of ice thickness products such as Bedmap and BedMachine, along with velocity maps including MEaSUREs and ITS_LIVE. Our analysis focuses on how the selection and quality of input datasets, especially the accuracy and location of thickness and velocity data along the flux gate, influence discharge and mass balance estimates. The study foucses on Basin 13 and its major outlet glaciers, with a primary emphasis on uncertainty assessment and the analyzing dynamic changes over time.

2. Study area

Wilkes Land, located in East Antarctica, stretches from Cape Hordern at 100°31′E to Point Alden at 142°02′E (Alberts, 1995). It overlies the Aurora Subglacial Basin and is often referred to as East Antarctica's weak underbelly (Stokes et al., 2022). This study focuses on analyzing mass balance uncertainties in this region. Figure 1 presents the study area. Wilkes Land is highlighted in the inset map, while the main map shows the drainage basins used in our calculations. Two types of basin boundaries are displayed in Figure 1. The first, based on ICESat data, includes 27 basins (Zwally et al., 2012). Basin 13, which primarily covers Wilkes Land, is selected for regional-scale uncertainty analysis. To better capture detailed glacier and ice shelf dynamics, we also use subregions defined by Rignot et al., (2019) to construct a long-term discharge time series. From these, five key subregions containing major outlet glaciers were selected to analyze discharge trends and assess uncertainties related to ice velocity and thickness data.

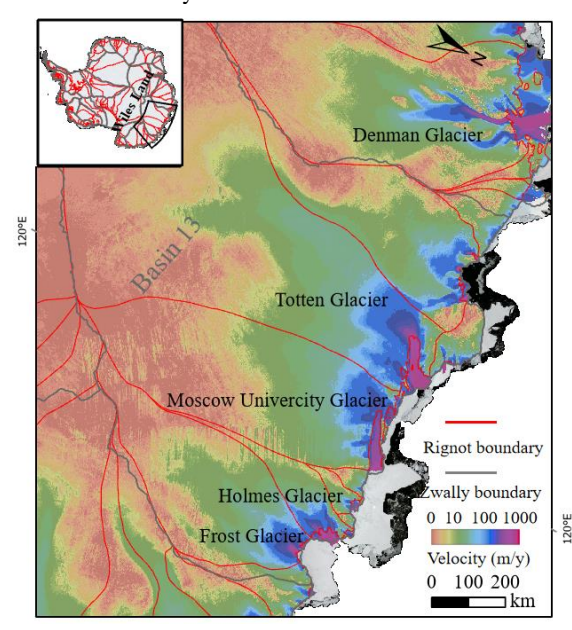


Figure 1. Location of Wilkes Land and drainage basin boundaries based on Zwally et al. (2012) and Rignot et al. (2019). The background shows the velocity map from MEaSUREs (Rignot, 2017).

3. Data and methods

3.1 Ice thickness

In this study, we use five ice thickness data to generate a new flux gate and analyze how thickness data influence the uncertainty of ice discharge estimates. The thickness datasets employed are summarized in Table 1. These include four gridded TIFF products as well as RES measurement data. The gridded datasets are Bedmap2, Bedmap3, BedMachineV2, and BedMachineV3. We use these datasets to provide ice thickness values and assess discharge uncertainties arising from differences between them.

For the gridded products, Bedmap2 has a thickness resolution of 1 km, with its associated uncertainty product at 5 km resolution. Bedmap3 updates Bedmap2 by filling significant data gaps, particularly in the deep interior of East Antarctica and along the West Antarctic coastlines, with improved thickness and uncertainty resolutions at 500 m. Similarly, BedMachineV2 and V3 both offer thickness data at a 500 m resolution.

To generate a new flux gate located closer to the grounding line and containing most observed data, we based our design on the flux gate (FG2) from Gardner et al. (2018) and refined it using RES data from Bedmap1, Bedmap2, and Bedmap3. Since RES-derived thickness data require correction for firn air content, we applied firn air correction (FAC) using the GSFC-FDMv1.2.1 model (Medley et al., 2022), which calculates firn height changes over the AIS from 1980 to 2022. We applied the average FAC as a correction to the RES thickness, with the associated uncertainty represented by the standard deviation of FAC values. The final uncertainty in RES thickness was computed through error propagation.

Dataset	Resolution	Format	Data source
Bedmap2	1 km/5 km	Grid tiff	Fretwell et al., 2022
Bedmap3	500 m	Grid tiff	Pritchard et al., 2024
BedMachineV2	500 m	Grid tiff	Morlighem et al., 2020
BedMachineV3	500 m	Grid tiff	Morlighem, 2022
RES	_	CSV	Bedmap1 Bedmap2 Bedmap3 Gardner et al., 2018

Table 1. Thickness data used in our study

3.2 Ice velocity

The velocity datasets used in this study are listed in Table 2 and include four types of velocity maps. The MEaSUREs multi-year velocity maps of the AIS (Rignot et al., 2022) are derived from satellite radar interferometry and cover the period from 1995 to 2022, with a spatial resolution of 450 m. We selected three representative periods from this dataset: 1995 to 2001, 2007 to 2009, and 2020 to 2022, to construct a long-term discharge time series.

The ITS_LIVE dataset (Gardner et al., 2019) provides higherresolution annual velocity maps from 1985 to 2022, mainly based on Landsat optical imagery. It includes two versions: Version 1 with a resolution of 240 m and Version 2 with 120 m. After evaluating both, we found that Version 2 has higher uncertainties in several key areas. Therefore, we used Version 1 in our discharge calculations. Since this version only extends to 2018, and considering the improved availability of high-quality Landsat-7 and Landsat-8 imagery after 2013, we selected ITS_LIVE annual maps from 2013 to 2018 for this study.

To extend the discharge series beyond 2018, we incorporated MEaSUREs annual velocity maps from 2019 and 2020. To address data gaps and high-uncertainty regions in the selected MEaSUREs and ITS_LIVE datasets, we first filled missing values using velocity maps from the closest time periods. Additionally, we used the MEaSUREs InSAR-based Antarctica velocity map, which combines observations from 1996 to 2016 and offers wide spatial coverage and consistent quality.

Dataset	Time span	Resolution	
MEaSUREs	1996.1.1-	450 m	
(Rignot, 2017)	2016.12.31		
MEaSUREs	1995.7.1-2001.6.30	450 m	
(Rignot et al., 2022)	2007.6.1-2009.7.30		
(Righot et al., 2022)	2020.6.1-2022.7.30		
MEaSUREs	2019.6.1-2020.7.30	1 km	
(Mouginot et al., 2017)	(Annual)	1 KIII	
ITS_LIVE	2013-2018 (Annual)	240 m	
(Gardner et al., 2019)	2013-2018 (Allilual)	240 111	

Table 2. Ice velocity data used in our study

3.3 Surface mass balance

Surface mass balance (SMB) is calculated as the total precipitation (including snow and rain) minus sublimation, drifting snow transport and erosion, and the runoff of meltwater that is neither retained nor refrozen (Van Wessem et al., 2018). SMB can be derived from regional climate models, such as RACMO2.3p1 and RACMO2.3p2, or from reanalysis datasets like ERA-5. However, reanalysis products typically only include precipitation and sublimation, and lack components that account for liquid water processes, such as meltwater runoff. Therefore, researchers generally rely on outputs from regional climate models to estimate SMB (Gardner et al., 2018; Rignot et al., 2019).

Compared to RACMO2.3p2, Rignot et al. (2019) found that RACMO2.3p1 produces balance velocities that align more closely with observations. Based on this finding, we adopt SMB values from RACMO2.3p1, following the approach of previous studies. This model covers the period from 1979 to 2014, with a spatial resolution of 27 km. To reduce variability in SMB and its influence on uncertainty analysis, we use the average SMB from 1995 to 2014 for discharge corrections and input estimates. Uncertainty in SMB is derived from the bias and bias uncertainty values provided by observational data across different elevations, as reported by Van Wessem et al. (2014, 2018).

3.4 Mass balance estimation

The mass balance calculated using the input-output (IO) method is estimated by subtracting ice discharge from surface mass balance (SMB). In this approach, SMB represents the input component and is obtained from regional climate models, while discharge represents the output component and is computed as the flux of ice across the grounding line. In this study, we adopt the grounding line provided by Gardner et al. (2018). Although RES provides the most accurate measurements of ice thickness, RES data are often sparse near the grounding line.

To improve the accuracy of thickness estimates, some studies have shifted the flux gate inland to locations with denser RES coverage. For example, Gardner et al. (2018) selected flux gate positions further upstream to include more RES measurements, even at the expense of proximity to the grounding line. The flux between the grounding line and the inland flux gate is then adjusted using mass conservation principles, typically involving SMB and basal melt rates. Since SMB corrections generally account for approximately 95% of the total adjustment, only SMB-based corrections are applied in this study.

The total discharge *D* is calculated as:

$$D = F + Corr_{GL-FG} \tag{1}$$

where $Corr_{GL-FG}$ is the SMB-based correction between the grounding line and the flux gate, and F is the flux across the new flux gate. The flux F is calculated as:

$$F = \sum_{i=1}^{n} gH_i (V_{x_i} W_{x_i} + V_{y_i} W_{y_i})$$
 (2) where H_i is the ice thickness at the *i*th point along the flux gate,

where H_i is the ice thickness at the *i*th point along the flux gate, g is the density of ice (assumed to be 917 kg/m³), V_{x_i} and V_{y_i} are the x and y components of ice velocity, and W_{x_i} and W_{y_i} represent the corresponding projected distances between adjacent gate segments. The total number of flux gate segments is denoted by n.

3.5 Uncertainty estimation

The uncertainty in mass balance is calculated through error propagation, as shown in equation (3):

$$\sigma_{MB} = \sqrt[2]{\sigma_{SMB}^2 + \sigma_D^2} \tag{3}$$

Here, σ_{SMB} represents the uncertainty in SMB, which is derived from the bias relative to in situ observations (Van Wessem et al., 2014, 2018). The uncertainty in discharge σ_D , is calculated as:

$$\sigma_D = \sqrt[2]{\sigma_F^2 + \sigma_{Corr_{GL-FG}}^2} \tag{4}$$

where $\sigma_{Corr_{GL-FG}}$ is the uncertainty associated with the SMB-based correction between the grounding line and the flux gate. The uncertainty in the flux term σ_F is estimated as the sum of uncertainties at individual segments (σ_{F_i}) along the flux gate:

$$\sigma_{F_i} = g \sqrt[2]{\frac{\left(W_{x_i}^2 + W_{y_i}^2\right)H_i^2}{2}\sigma_{V_i}^2 + \left(V_{x_i}W_{x_i} + V_{y_i}W_{y_i}\right)^2\sigma_{H_i}^2}$$
 (5)

where σ_{V_i} and σ_{H_i} represent the uncertainties in velocity and ice thickness at the *i*th point, respectively.

4. Results

4.1 New flux gate around the Wilkes Land

Based on the FG2 dataset and RES measurements from Bedmap1, Bedmap2, and Bedmap3, we generated a new flux gate dataset, referred to as FG. The updated FG is shown in Figure 2. Compared to FG2, the new flux gate is positioned closer to the grounding line. Bedmap3 provides denser RES coverage in the

Wilkes Land region, filling previous data gaps and enabling the construction of a more accurately positioned flux gate. The original FG2 flux gate lies up to approximately 61 km inland from the grounding line, with an average offset of \sim 15 km in Basin 13. In contrast, our revised flux gate reduces the average offset by about 7 km, bringing it significantly closer to the grounding line.

Using this new flux gate, we calculate discharge based on five different ice thickness datasets: (1) Bedmap2 (BMP2); (2) Bedmap3 (BMP3); (3) BedMachineV2 (BM2); (4) BedMachineV3 (BM3); (5) a hybrid dataset (BMP3_RES) using RES measurements where available, and Bedmap3 to fill the remaining gaps. The average thickness and associated uncertainty along the flux gate in the Wilkes Land region are as follows: BMP2: 702 ± 615 m; BMP3: 681 ± 16 m; BM2: 668 ± 51 m; BM3: 670 ± 48 m; BMP3_RES: 665 ± 12 m. These results indicate a clear reduction in uncertainty for BMP3 and BMP3_RES compared to earlier products, highlighting the improved data quality of Bedmap3 and the effectiveness of incorporating RES measurements.

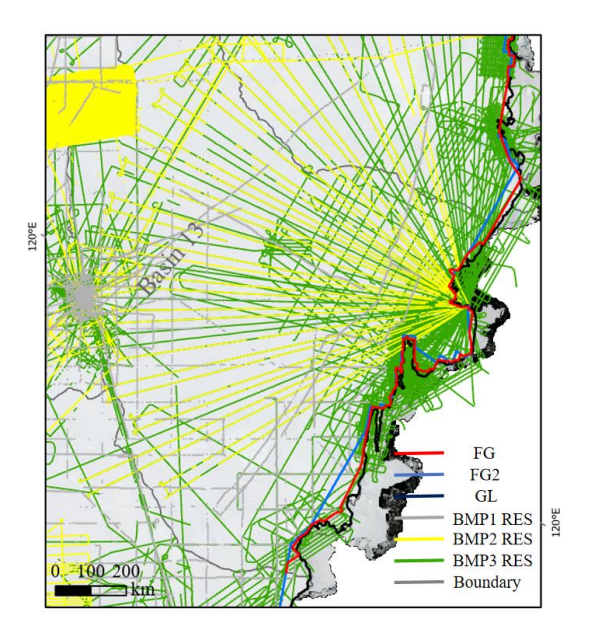


Figure 2. Distribution of RES measurements and flux gate locations. Light grey lines represent RES data from Bedmap1, yellow lines from Bedmap2, and green lines from Bedmap3. The newly generated flux gate (FG) is shown in red, while the previous flux gate (FG2) is shown in blue. The grounding line is indicated in black. The background image is the LIMA mosaic (Bindschadler et al., 2008).

4.2 Discharge trends and uncertainty analysis in basin 13

Basin 13 is the primary drainage basin in Wilkes Land, encompassing major outlet glaciers such as Totten Glacier, Moscow University Glacier, and Holmes Glacier. This basin contributes the highest discharge (~220 Gt/year) among all 27 Antarctic basins (Gardner et al., 2018; Shen et al., 2018). In this study, we generate five long-term discharge time series spanning from 1995 to 2022, using five different ice thickness datasets (BMP2, BMP3, BM2, BM3, and BMP3_RES) and ten velocity maps corresponding to the following periods: 1995–2001, 2007–2009, 2013, 2014, 2015, 2016, 2017, 2018, mid-2019 to mid-2020, and mid-2020 to mid-2022.

Figure 3 presents two representative discharge time series selected from the five. One shows the highest uncertainty, and the other the lowest. Figure 3 (a) displays results based on BMP2. Due to the high uncertainty in Bedmap2 thickness data, the corresponding discharge estimates have large uncertainty, averaging 223±112 Gt/y from 1995 to 2022. This result is comparable to values reported by Gardner (226 Gt/y in 2008; 223 Gt/y in 2015), though the uncertainty remains too large for robust interpretation. In contrast, Figure 3 (b) shows results derived from the BMP3_RES dataset, which combines RES measurements with Bedmap3 thickness data in regions lacking RES coverage. This dataset has the lowest mean thickness uncertainty (665±12 m) among the five tested, yielding an average discharge of 219±15 Gt/y. The visibly shorter error bars in Figure 3(b) compared to Figure 3(a) underscore the significant impact of ice thickness accuracy on discharge uncertainty. From Figure 3 (b), we observe that the discharge remained consistently high (~220 Gt/year) throughout the study period. A slight increasing trend is evident from 1995 to 2017, although this trend is within the uncertainty range. Between 2018 and 2020, a temporary drop below the average is observed, followed by a return to near-average values during 2020-2022.

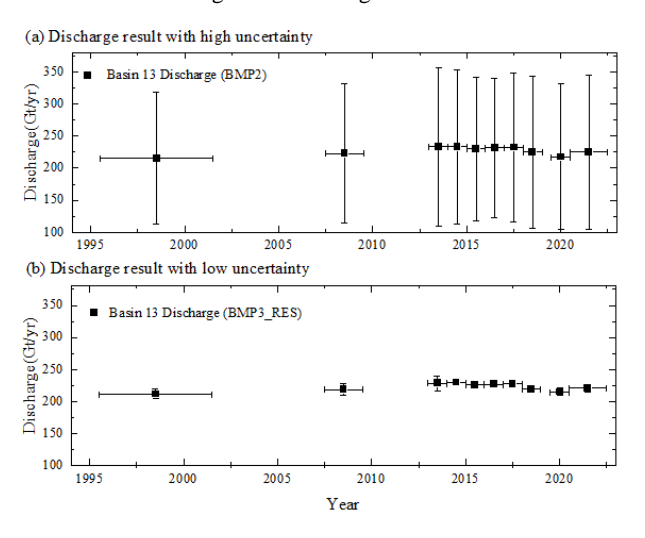


Figure 3. Long-term discharge trends in Basin 13, illustrating differences in uncertainty between datasets with high (BMP2) and low (BMP3_RES) thickness uncertainty.

To assess the impact of ice thickness and velocity data on discharge uncertainty, we calculate the uncertainty percentage as the ratio of discharge uncertainty to discharge. Figure 4 shows the uncertainty percentages across different thickness datasets and velocity maps. Among the five thickness datasets, BMP2 exhibits the highest uncertainty percentage (53%), while the other four datasets show substantially lower values (~10%). BMP3 performs best among the gridded datasets, with uncertainty only slightly higher (~1%) than BMP3_RES. Regarding the velocity maps, we find a variation of approximately 8% in discharge uncertainty percentage across the ten velocity periods. With the improved flux gate, the overall discharge uncertainty in Basin 13 is reduced from 53% to 4%. Of this improvement, approximately 42% is attributed to enhanced ice thickness data, and about 7% is due to improved velocity observations.

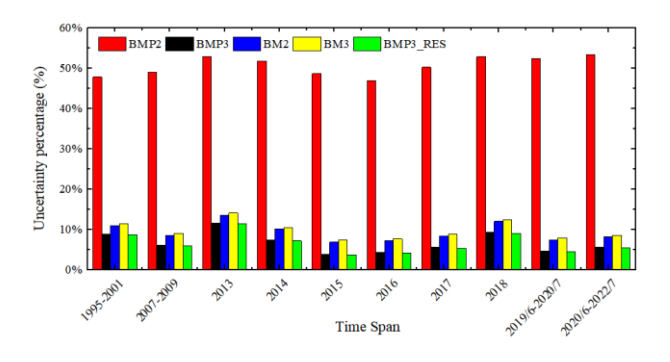


Figure 4. Discharge uncertainty percentage for the five ice thickness datasets and ten velocity map periods from 1995 to 2022.

4.3 Discharge trend of the main glacier regions

In Wilkes Land, there are many outlet glaciers. In this study, we selected five major glacier catchments to analyze their discharge trends. The estimated results are shown in Figure 5. This figure presents two of the five long-term discharge series: one based on BMP2 and the other on BMP3_RES. A clear improvement in uncertainty is observed when using BMP3_RES compared to BMP2. The Totten catchment has the highest discharge among the selected subregions, with an average of approximately 70 ± 5 Gt/y for BMP3 RES and 70 ± 11 Gt/y for BMP2 during the period from 1995 to 2022. These values are consistent with the results of Rignot et al. (2019), who reported a discharge of 71 Gt/y from 2009 to 2017. Although there are short-term fluctuations suggesting a possible increasing trend, the variations remain within the uncertainty range. The Moscow subregion shows a relatively stable discharge of about 42 Gt/y throughout the study period. The Denman, Frost, and Holmes subregions exhibit an increasing discharge trend during the period from 1995 to 2022. This trend may be related to enhanced intrusion of Circumpolar Deep Water (CDW) and structural damage to the ice shelves in these areas.

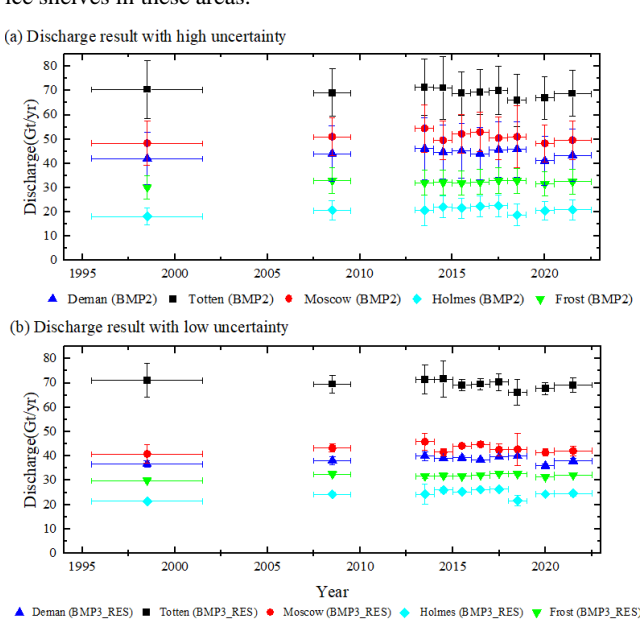


Figure 5. Long-term discharge trends for the Denman, Totten, Moscow, Holmes, and Frost subregions, and comparison of uncertainties associated with different thickness datasets

4.4 Mass balance analysis

Mass balance is calculated as the difference between surface mass balance (SMB) and ice discharge. To minimize the influence of SMB variability on our uncertainty analysis, we apply a time-averaged SMB value (1995–2014) across the entire time series. The mass balance results for Basin 13 are presented in Table 3. This table includes five discharge time series derived from different ice thickness datasets; however, due to its lowest associated discharge uncertainty, only the mass balance based on the BMP3_RES thickness dataset is reported. Basin 13 exhibits a relatively high average ice discharge of approximately 219 Gt/y between 1995 and 2022. Although this dynamic outflow is partially compensated by SMB input averaging 208 Gt/y, the region still undergoes net mass loss during certain periods. Over the full study period, the mean mass balance of Basin 13 is estimated at -11 ± 20 Gt/y.

5. Conclusions

In this study, we developed an updated flux gate (FG) product for the Wilkes Land region by incorporating improved radio-echo sounding (RES) data coverage from Bedmap1, Bedmap2, and Bedmap3. These enhancements significantly reduced data gaps near the grounding line. Compared with the previous FG2 dataset, the new FG reduced the average distance from the grounding line to approximately 7 km. Using this improved flux gate, we assessed long-term ice discharge trends in Basin 13 and its major glacier catchments over the period from 1995 to 2022. We applied five different ice thickness datasets to evaluate their influence on discharge estimates and associated uncertainties. Among these, the BMP3_RES dataset, which integrates RES measurements with Bedmap3 data, produced the lowest mean uncertainty, about 12 m in ice thickness and 15 Gt/y in discharge This result highlights the essential role of accurate ice thickness data in reducing uncertainty in discharge estimation.

The combination of the updated flux gate and enhanced input datasets reduced discharge uncertainty from 53% to 4%. Approximately 42% of this improvement resulted from better thickness data, while about 7% was due to the use of improved velocity datasets. Subregional analysis showed that Totten Glacier remained the largest contributor to ice discharge in Wilkes Land, with an average of around 70 Gt/y, which is consistent with previous research. The discharge from Moscow Glacier remained relatively stable throughout the study period. The Denman, Holmes, and Frost glaciers show slight increasing discharge trends, likely driven by oceanic processes such as modified Circumpolar Deep Water intrusion and weakening of their ice shelves.

T:	Discharge				SMB	MB	
Time span	BMP2	BMP3	BMV2	BMV3	BMP3_RES	(1995-2014)	(BMP3_RES)
1995-2001	215±103	213±19	209±23	209±24	212±18	208±12	-4 ±22

2007-2009	223±109	221±13	215±18	216±19	219±13	208±12	-11 ±18
2013	234±124	231±27	227±31	226±32	229±26	208±12	-20 ±29
2014	233±121	232±17	227±23	227±24	230±16	208±12	-22 ±21
2015	230±112	228±9	222±15	223±16	226±8	208±12	-18 ±15
2016	232±109	229±10	223±16	224±17	227±9	208±12	-19 ±15
2017	232±117	230±13	225±19	225±20	228±12	208±12	-20 ±17
2018	225±119	221±21	216±26	216±27	219±20	208±12	-11 ±23
2019/6-2020/7	217±114	217±10	211±15	212±17	215±10	208±12	-7 ±16
2020/6-2022/7	225±120	223±13	217±18	218±19	221±12	208±12	-13 ±17

Table 3. Mass balance results between 1995 and 2022

Acknowledgements

We gratefully acknowledge the institutions and research teams whose data products made this study possible. The Bedmap2 and Bedmap3 datasets were provided by the British Antarctic Survey (BAS). BedMachineV2 and BedMachineV3 from the National Snow and Ice Data Center (NSIDC). Ice velocity maps from the ITS_LIVE project were provided by the National Aeronautics and Space Administration (NASA), and additional velocity products were obtained from NASA's MEaSUREs Program via NSIDC. Surface mass balance and climate forcing data were derived from the RACMO model, developed by the Royal Netherlands Meteorological Institute (KNMI) and Utrecht University. Firn air content estimates were obtained from the GSFC-FDMv1.2.1 model, developed at NASA Goddard Space Flight Center. This work was supported by the National Key Research and Development Program of China (Grant No. 2021YFB3900105).

References

Adusumilli S, Fricker H A, Medley B, Padman L, Siegfried M R. 2020. Interannual variations in meltwater input to the Southern Ocean from Antarctic ice shelves. *Nature Geoscience*, 13: 616-620

Alberts F.G. 1995. Geographic names of the Antarctic. *National Science Foundation*.

Bindschadler R, Vornberger P, Fleming A, Fox A, Mullins J, Binnie D, Paulsen S J, Granneman B, Gorodetzky D. 2008. The Landsat image mosaic of Antarctica. *Remote Sensing of Environment*, 112: 4214-4226

Cheng Y, Hai G, Cui X, Lv D, Qiao G, Li R. 2023. Mass balance of the Antarctic Ice Sheet from 2013 to 2018 estimated using the input-output method with updated remote sensing products. *Science China Earth Sciences*, 66: 1478-1492

Fretwell P, Pritchard H, Vaughan D, Bamber J, Barrand N, Bell R E, Bianchi C, Bingham R, Blankenship D, Casassa G. 2022. BEDMAP2-Ice thickness, bed and surface elevation for Antarctica-gridding products. (*No Title*):

Gardner A S, Fahnestock M A, Scambos T A. 2019. ITS_LIVE regional glacier and ice sheet surface velocities. *Data archived at National Snow and Ice Data Center*, 10:

Gardner A S, Moholdt G, Scambos T, Fahnstock M, Ligtenberg S, Van Den Broeke M, Nilsson J. 2018. Increased West Antarctic and unchanged East Antarctic ice discharge over the last 7 years. *The Cryosphere*, 12: 521-547

Li R, Cheng Y, Chang T, Gwyther D E, Forbes M, An L, Xia M, Yuan X, Qiao G, Tong X. 2023. Satellite record reveals

1960s acceleration of Totten Ice Shelf in East Antarctica. *Nature Communications*, 14: 4061

Li R, Li G, Hai G, Xie H, Cheng Y, Chen W, Cui X, Ding M, Gao C, Hao T. 2024. Reconciled estimation of Antarctic ice sheet mass balance and contribution to global sea level change from 1996 to 2021. *Science China Earth Sciences*, 67: 3562-3578

Medley B, Neumann T A, Zwally H J, Smith B E, Stevens C M. 2022. Simulations of firn processes over the Greenland and Antarctic ice sheets: 1980–2021. *The Cryosphere*, 16: 3971-4011

Morlighem M, Rignot E, Binder T, Blankenship D, Drews R, Eagles G, Eisen O, Ferraccioli F, Forsberg R, Fretwell P. 2020. Deep glacial troughs and stabilizing ridges unveiled beneath the margins of the Antarctic ice sheet. *Nature Geoscience*, 13: 132-137

Morlighem M. 2022. 2. MEaSUREs BedMachine Antarctica, Version 3. NASA National Snow and Ice Data Center Distributed Active Archive Center. (DAAC) data set

Mouginot J, Scheuchl B, Rignot E. 2017. MEaSUREs annual Antarctic ice velocity maps, version 1. NASA National Snow and Ice Data Center Distributed Active Archive Center (DAAC) data set

Otosaka I N, Shepherd A, Ivins E R, Schlegel N, Amory C, van den Broeke M R, Horwath M, Joughin I, King M D, Krinner G. 2023. Mass balance of the Greenland and Antarctic ice sheets from 1992 to 2020. *Earth System Science Data*, 15: 1597-1616

Pritchard H D, Fretwell P T, Fremand A C, Bodart J A, Kirkham J D, Aitken A, Bamber J, Bell R, Bianchi C, Bingham R G. 2025. Bedmap3 updated ice bed, surface and thickness gridded datasets for Antarctica. *Scientific Data*, 12: 414

Pritchard H, Fretwell P, Fremand A, Bodart J, Kirkham J, Aitken A, Bamber J, Bell R, Bianchi C, Bingham R. 2024. BEDMAP3-Ice thickness, bed and surface elevation for Antarctica-gridding products.:

Rignot E. 2017. Measures InSAR-based Antarctica ice velocity map, version 2. *Nat. Snow Ice Data Center*:

Rignot E, Mouginot J, Scheuchl B, Jeong S. 2022. Changes in Antarctic ice sheet motion derived from satellite radar interferometry between 1995 and 2022. *Geophysical Research Letters*, 49: e2022G-e100141G

Rignot E, Mouginot J, Scheuchl B, Van Den Broeke M, Van Wessem M J, Morlighem M. 2019. Four decades of Antarctic Ice Sheet mass balance from 1979–2017. *Proceedings of the*

National Academy of Sciences, 116: 1095-1103

Shen Q, Wang H, Shum C K, Jiang L, Hsu H T, Dong J. 2018. Recent high-resolution Antarctic ice velocity maps reveal increased mass loss in Wilkes Land, East Antarctica. *Scientific Reports*, 8: 4477

Shepherd A, Ivins E, Rignot E, Smith B, van den Broeke M, Velicogna I, Whitehouse P, Briggs K, Joughin I, Krinner G. 2018. Mass balance of the Antarctic Ice Sheet from 1992 to 2017. *Nature*.

Smith B, Fricker H A, Gardner A S, Medley B, Nilsson J, Paolo F S, Holschuh N, Adusumilli S, Brunt K, Csatho B. 2020. Pervasive ice sheet mass loss reflects competing ocean and atmosphere processes. *Science*, 368: 1239-1242

Stokes C R, Abram N J, Bentley M J, Edwards T L, England M H, Foppert A, Jamieson S S R, Jones R S, King M A, Lenaerts J T M, Medley B, Miles B W J, Paxman G J G, Ritz C, van de Flierdt T, Whitehouse P L. 2022. Response of the East Antarctic Ice Sheet to past and future climate change. *Nature*, 608: 275-286

Van Wessem J M, Reijmer C H, Morlighem M, Mouginot J, Rignot E, Medley B, Joughin I, Wouters B, Depoorter M A, Bamber J L. 2014. Improved representation of East Antarctic surface mass balance in a regional atmospheric climate model. *Journal of Glaciology*, 60: 761-770

Van Wessem J M, Van De Berg W J, Noël B P, Van Meijgaard E, Amory C, Birnbaum G, Jakobs C L, Krüger K, Lenaerts J T, Lhermitte S. 2018. Modelling the climate and surface mass balance of polar ice sheets using RACMO2–Part 2: Antarctica (1979–2016). *The Cryosphere*, 12: 1479-1498

Zwally H J, Giovinetto M B, Beckley M A, Saba J L. 2012. Antarctic and Greenland drainage systems, *GSFC cryospheric sciences laboratory*.